Postprint of: Włodarski W., A model development and experimental verification for a vapour microturbine with a permanent magnet synchronous generator, Applied Energy, Vol. 252 (2019), 113430, DOI: 10.1016/j.apenergy.2019.113430

A model development and experimental verification for a vapour microturbine with a permanent magnet synchronous generator

Wojciech Włodarski

Gdansk University of Technology, Faculty of Mechanical Engineering, Department of Energy and Industrial Apparatus, Narutowicza 11/12, 80-233 Gdansk, Poland

Abstract

Vapour microturbines with permanent magnet synchronous generators are implemented in micropower plants for dispersed power generation systems. The dynamic model of such a microturbine set was developed and presented. The developed relations result from the generic equations. Experimental data for two different working medium were used for model verification. A microturbine set model was tested during the changes in the parameters of a working medium or an electrical load. Examples of a comparison between the experimental results and simulations are shown and discussed. The developed model ensures comparable accuracy as gas microturbine models found in the literature. In the case of vapour microturbine sets, in addition to accuracy, provides a larger area of operation. An operation during a start-up process was also analysed. Due to model simplifications, the accuracy decreases for a start-up operation from a cold state. The developed model can be a useful tool for some engineering applications or for studying the various operational aspects of vapour microturbines with permanent magnet synchronous generators.

Keywords: Micro power generation, Microturbines, Microturbine dynamics, Simulations

Email address: wwlodar@pg.edu.pl (Wojciech Włodarski)

1. Introduction

Distributed energy systems are decentralized, modular and flexible technology. They ensure the improvement of local security of energy supply and complement the centralized energy system [1]. These systems can comprise multiple generation and storage components [2]. In distributed power engineering, micropower plants are used for the local production of electric power and heat or for heat utilization [3]. In many cases, the microscale introduces construction and technological problems. Within the development of micro power plants, two research areas can be indicated: compact heat exchangers and micro-engines, which play a significant role in the process of energy conversion.

Micro heat exchangers are developed in many ways. Techniques for intensifying heat transfer in plate heat exchangers are applied [4] or compact heat exchangers are built based on minichannels [5], microchannels [6] or helical coiled tubes [7]. It is also proposed to apply a jet technology in heat exchangers dedicated to micro combined heat and power units. An innovative solution in this area is a microjet heat exchanger with a cylindrical structure, over which intensive experimental [8] and numerical [9] work is carried out.

In the case of engines, volumetric and turbine engines are developed in parallel. As examples of the use of volumetric engines, it can indicate rotary vane expanders described in Refs. [10] and [11], scroll expanders [12] or single-screw expanders [13]. Ref. [14] deals with the comparison of the volumetric expanders and proposes a procedure for such device selection. Both axial [15] and radial microturbines [16] are applied. It should be mentioned that viscous bladeless turbines are also considered [17]. An extensive review of this issue can be found in [18].

Power generation systems with microturbine sets, consisting of an electric generator driven by thermal microturbine, are developing. They can be one of the components of mini/micro-grids [19], which are electrical systems that serve diverse users and can be interconnected and interact with the main utility grid or operate independently based on distributed energy generation [20]. For this purpose, both gas [21] and steam [22] microturbines are used. Modifications of gas microturbines with the combustion chamber at the turbine outlet or the special air by-pass system of the combustor are introduced [23]. Microturbines have also found applications in poly-generation [24] and combined [25] power systems. When an electric power generation is based on low-temperature heat sources (for example, geothermal [26], ocean

[27] or waste heat recovery systems [28]), the vapour microturbines cooperate with installations in which the ORC (Organic Rankine Cycle) [29], or OFC (Organic Flash Cycle) [30] is executed. It should be pointed out that also the innovative pumpless systems, driven by the low-temperature heat sources [31], are developing. Recently, with the intensive development of the distributed energy sector in the European Union, ORC/OFC technology is perceived as a prospective technology for household scale micro-cogeneration systems [32].

Microturbine sets are already offered by many companies from the energy market. However, research activities are still in progress to improve the efficiency (e.g. by placing special attention on the designing of the blade cascades, both for axial [33], [34] and radial [35] turbines), solve control [36] or bearing [37] problems and to decrease investment costs [38]. Difficulties are also connected with miniaturisation, high rotational speed and reliability. Microturbines are designed to have a compact structure and small volume, which makes them more susceptible to internal leakages [39].

A microturbine set is usually designed for operation in specified conditions, i.e. at the specified thermodynamic parameters of a working medium and specified electric load. A set of these parameters bears the name of design or calculation parameters. However, during an operating lifetime, a microturbine set can work in differing conditions, for example, due to a change of working medium parameters or electric load. In such conditions, a set can work at partial load or overload, rotational speed also can change. Not all of the above changes are permissible for example, due to strength reasons, durability of generator armature winding or the required values of voltage and current intensity. A possibility of operation in such conditions should be taken into account.

Valuable information about microturbine set operation may be provided by experimental work. Unfortunately the published results, of experimental examination, usually refer to steady-state microturbine operation (for gas and vapour microturbines, the tests described in [40] and [41] can be indicated respectively). Changes in operating parameters can also take a dynamic course (for instance, as a result of connecting or disconnecting electric energy receivers). Research work on microturbine sets operation in dynamically changing conditions, in particular, based on experimental results, are rare. Tests performed on the gas microturbine can be found in [42]. Experimental investigations of vapour microturbines, in transient operating conditions, are described in [43] (for axial type turbine) and [44] (for radial type turbine).

The dynamic process examination of the ORC system is also presented in [45].

A mathematical model of a microturbine set is required to analyze the above mentioned impacts. This is of great practical importance, for example, in a case of designing of a control system. There are some works describing a control of turbine sets, but most of them concern on steam or gas turbines of high power or gas microturbines, which makes it difficult to draw conclusions about vapour devices with low power. The regulation of microturbines is not comprehensively addressed in the literature. Works focussing on vapour microturbine control are extremely rare [46] and usually concern transfers "macro" scale solutions to "micro" devices. Determining an appropriate solution for a control system requires analysis and simulation tests based on a mathematical model of a device.

The modelling of gas microturbines is extensively described in bibliography. Such models differ in the degree of complexity and practical application in simulation research. Full-order models are developed, such as those described in Refs. [47] and [48], where thermodynamic relations are based on physical principles. Higher order models which integrate thermodynamic relations with those describing power electronic converters can be found in Refs. [49] and [50]. When the high order models seem too complex for simulation applications, simplified relations are implemented. Among the simplified modelling, differ approaches can be indicated: the reduction techniques based on the time decoupling concept [51], applying approximations [52], the reduction of the number of necessary parameters [53] and the input-output based methods treating the gas microturbine as a black box [54].

There are very little works in the literature with vapour microturbine sets models. Available vapour microturbine models often do not include cooperation between a turbine and a generator [55]. The model of a vapour microturbine set can be found in [56]. This is an empirical model with the structure determined by observed relations among experimental data. The model adopts the linear relation between a load resistance and a rotational speed. In fact, this relation is nonlinear. As a result, the mentioned model can ensure an acceptable accuracy for operation with relatively small changes in electric load. It can be expected that in a case of small power systems (for example, an individual household), an electricity demand may dynamically change. Switching on a single device or several devices at the same time can produce a peak demand of several kilowatts [57]. In addition, this model assumes a constant pressure value after a turbine. This pressure, dur-

ing operation, may change, for example after change condenser operating conditions.

For these reasons, it seems necessary to develop a mathematical model that would allow calculating an operating state of a vapour microturbine set in a relatively wide range of electric load and pressure of a working medium. Such a model should also enable analyzing on an operation of microturbine sets in transient states. It should be verified by comparing simulation results with experimental data, preferably on a complete set consisting of cooperating a microturbine and a generator. Then, it would be a useful tool for studying various operational aspects or for some engineering applications. A literature survey indicates that there is limited research available on this topic.

The major objective of this study is to fill the research gap and investigate if the above-mentioned requirements can be achieved. Below are the major contributions and novelties of this study:

1. Generic equations of a turbine and permanent magnet synchronous generator (PMSG) were used to develop the new model of a vapour microturbine set. The model enables analysis in both steady and unsteady conditions. The considered set cooperates with a diode rectifier, but it is possible to integrate the proposed model with another system.
2. Developed relations were simplified to such a form that the values of the model coefficients can be easily determined based on the results of an experimental examination.
3. The model has been verified using the results of unique experimental research. The uniqueness of these results consists in the fact that under laboratory conditions, various expected operating states were simulated (for the example step changes of the electrical load or start-up operation) and they were made with two different working medium. The results of such vapour microturbine set studies have not yet been published.
4. It has been found that neglecting a thermal state of the vapour microturbine can lead to inaccuracies in the simulation, e.g. in a start-up operation from a cold state.

The paper is organized as follows: Section 1 is the introduction, Section 2 describes the studied set and develops its mathematical model, Section 3 and Section 4 present the results and discussion of the model verification, Section 5 draws the conclusions.

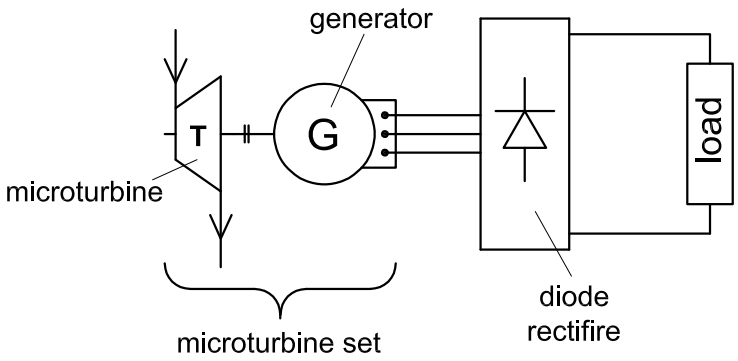

Figure 1: A schematic diagram of a vapour microturbine with a permanent magnet synchronous generator and a diode rectifier

2. A model of a vapour microturbine set

The scheme of a considered microturbine set is shown in Fig. 1. A microturbine set consists of a microturbine and a three-phase permanent magnet generator, connected with each other. A single stage axial microturbine is used. A generator is connected to a diode rectifier, which converts an alternating current into a direct current.

2.1. Steady state operation of a turbine

The schematic diagram of a microturbine is shown in Fig. 2. A working medium approaches a turbine at a pressure p_1 and a temperature T_1. A medium pressure after a turbine is p_2. A rotational speed of a rotor is n and a torque on a turbine shaft is M_T.

A turbine power can be calculated due to the following relation:

$$N = \eta \cdot m \cdot H_s \tag{1}$$

where: η denotes the turbine efficiency, m - medium mass the flow rate, H_s - turbine the isentropic enthalpy drop.

A turbine efficiency was described by a quadratic function:

$$\eta = a \cdot \nu - b \cdot \nu^2 \tag{2}$$

where: ν - velocity ratio, a,b - constants.

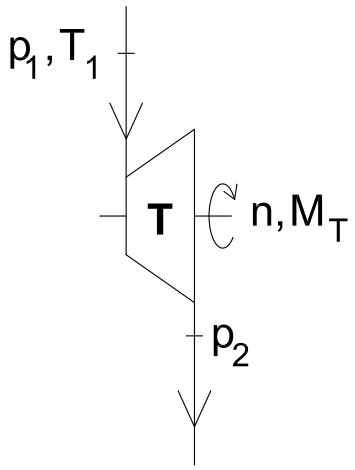

Figure 2: A schematic diagram of a vapour microturbine

The value of the velocity ratio is:

$$\nu = \frac{\omega r}{\sqrt{2H_s}} \tag{3}$$

where: ω - rotor angular speed, r - turbine stage mean radius. Taking this into account in equation (2) gives the following expression:

$$\eta = a\frac{\omega r}{\sqrt{2H_s}} - b\frac{(\omega r)^2}{2H_s} \tag{4}$$

Basing on the Stodola-Flugel formula, there is the following relation between a vapour flow rate and thermodynamic parameters before and after any change of a turbine flow:

$$m = m_0\sqrt{\frac{T_{10}}{T_1}}\sqrt{\frac{p_1^2 - p_2^2}{p_{10}^2 - p_{20}^2}} \tag{5}$$

where index 0 denotes the parameters before any turbine flow change.

Using the equations (1), (4), (5) we can write:

$$N_T = \left(a\frac{\omega r}{\sqrt{2H_s}} - b\frac{(\omega r)^2}{2H_s}\right) m_0\sqrt{\frac{T_{10}}{T_1}}\sqrt{\frac{p_1^2 - p_2^2}{p_{10}^2 - p_{20}^2}}H_s \tag{6}$$

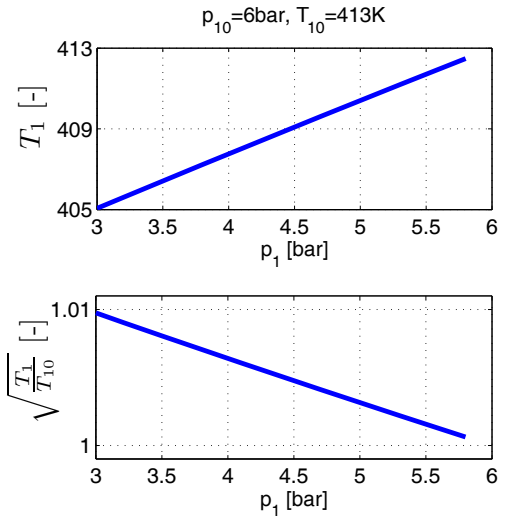

Figure 3: The temperature of the ethanol vapour T_1 as a function of pressure p_1, after the isenthalpic throttling process from pressure $p_{10} = 6\,bars$ and temperature $T_{10} = 413\,K$

It can be noticed that in typical turbines with superheated steam supply, after throttling the working medium in the control valve, the temperature at the turbine inlet changes to a relatively small extent. This phenomenon also occurs in many cases of vapour turbines. The example is shown in Fig. 3. The graph shows the temperature change of ethanol vapor, after the isenthalpic throttling process from the pressure of 6 bars and the temperature of 413 K (the values were taken from the RefProp database). The graph also shows how the $\sqrt{\frac{T_{10}}{T_1}}$ relationship value changes in this case. After reducing the pressure from 6 bars to 3 bars, the value of this relation increased by approximately 1 %.

If such inaccuracy is acceptable, it can be assumed that $\sqrt{\frac{T_{10}}{T_1}} \approx 1$. Then the relation (6) can be converted into the following form:

$$N_T = (k_1 \omega \sqrt{H_s} - k_2 \omega^2) \sqrt{p_1^2 - p_2^2} \tag{7}$$

where k_1, k_2 are turbine coefficients.

Then the relation for a torque on a turbine shaft can be obtained:

$$M_T = (k_1 \sqrt{H_s} - k_2 \omega) \sqrt{p_1^2 - p_2^2} \tag{8}$$

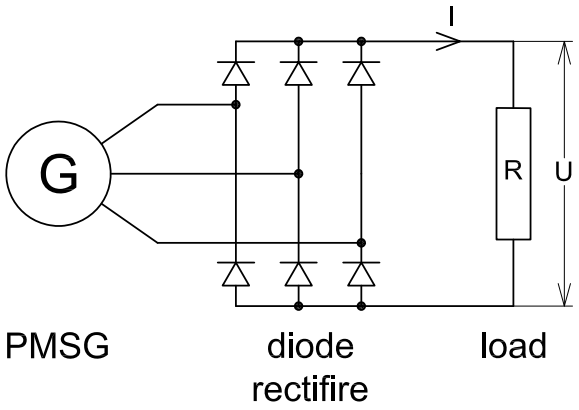

Figure 4: A schematic diagram of a permanent magnet synchronous generator assisted with a diode rectifier

If it was necessary to take into account the effect of the temperature changes, the power and torque of the turbine can be described as:

$$N_T = (k_3\omega\sqrt{H_s} - k_4\omega^2)\sqrt{\frac{p_1^2 - p_2^2}{T_1}} \tag{9}$$

$$M_T = (k_3\sqrt{H_s} - k_4\omega)\sqrt{\frac{p_1^2 - p_2^2}{T_1}} \tag{10}$$

where k_3, k_4 are turbine coefficients.

2.2. Steady state operation of a generator with a diode rectifier

The steady state model of a permanent magnet synchronous generator with a 6-pulse diode rectifier (Fig. 4) is presented. The system load is a resistor with R resistance. Output average DC voltage and current intensity are equal to U and I respectively.

The phase diagram of a single phase of a PMSG is shown in Fig. 5, where E is an induced electromotive voltage, R_s is a stator resistance, X_s is a synchronous reactance, and U_s and I_s are a phase voltage and phase current intensity. The corresponding equation can be expressed as:

$$E^2 = (U_s + I_s R_s)^2 + (X_s I_s)^2 \tag{11}$$

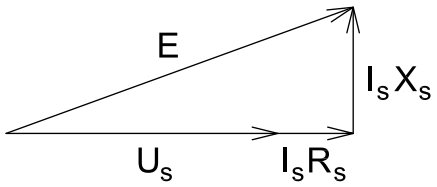

Figure 5: Phase vector diagram of a permanent magnet synchronous generator

Substituting $E = p\omega k_e$ and $X_s = p\omega L$ (where p is the number of magnet poles, k_e is the generator constant and L is a single phase inductance of a stator) into (11) yields:

$$(p\omega k_e)^2 = (U_s + I_s R_s)^2 + (p\omega L I_s)^2 \tag{12}$$

Ignoring the losses of a diode rectifier, the relation between an average voltage value at a DC side and phase voltage may be written as:

$$U_s = \frac{\pi U}{3\sqrt{6}} \tag{13}$$

The average current intensity value at a DC side can be expressed as:

$$I_s = \frac{\sqrt{6}}{\pi} I \tag{14}$$

Taking equations (13), (14) and $U = IR$ into equation (12) gives the following expression:

$$I^2 = \frac{(p\omega k_e)^2}{\left(\frac{\pi^2 R + 18 R_s}{3\sqrt{6}\pi}\right)^2 + \left(p\omega L \frac{\sqrt{6}}{\pi}\right)^2} \tag{15}$$

Due to the negligence of the losses in the rectifier, the power of the generator can be expressed as $N_E = I^2 R$ or:

$$N_E = \frac{R(p\omega k_e)^2}{\left(\frac{\pi^2 R + 18 R_s}{3\sqrt{6}\pi}\right)^2 + \left(p\omega L \frac{\sqrt{6}}{\pi}\right)^2} \tag{16}$$

Then the relation for an electromagnetic torque of a generator can be obtained:

$$M_E = \frac{R\omega(pk_e)^2}{\left(\frac{\pi^2 R + 18 R_s}{3\sqrt{6}\pi}\right)^2 + \left(p\omega L \frac{\sqrt{6}}{\pi}\right)^2} \tag{17}$$

2.3. Microturbine set modelling

In a steady state, a turbine torque should be equal to an electromagnetic torque of a generator:

$$M_T = M_E \tag{18}$$

Taking equations (8), (17) and (18) gives the following expression:

$$(k_1\sqrt{H_s} - k_2\omega)\sqrt{p_1^2 - p_2^2} = \frac{R\omega(pk_e)^2}{\left(\frac{\pi^2 R + 18R_s}{3\sqrt{6}\pi}\right)^2 + \left(p\omega L\frac{\sqrt{6}}{\pi}\right)^2} \tag{19}$$

Formula (19) presents the relation, in a steady state, between the thermodynamic parameters of a medium, a load resistance and an angular speed of a vapour microturbine set.

A microturbine set rotor motion may be described by the following differential equation:

$$J\frac{d\omega}{dt} = M_T - M_E \tag{20}$$

where J is a microturbine set rotor polar moment of inertia.

3. Model validation

The results of the experimental tests of the microturbine set were used for the model validation. Data for the two working medium were used: compressed air and vapour of ethanol. The set consists of the single-stage microturbine and permanent magnet generator. The turbine stage is an impulse type with an axial flow and partial admission. The turbine rotor and the generator rotor are mounted on one shaft. The set during test runs is shown in Fig. 6. Detailed information of the microturbine set and the laboratory test rig can be found in [58].

The data used to determine model coefficients for turbine operation with compressed air as a working medium are shown in Fig. 7. There are experimentally obtained relations between rotational speed, phase current intensity, phase-to-phase voltage and load resistance. The data for the vapour of the ethanol operation are shown in Fig. 8.

The generator phase stator resistance was measured. Its value (in the cold state) is $R_s = 1\,\Omega$.

Generator constant k_e and inductance L were calculated from equation 12 (taking into account the relationship $U_{LL} = \sqrt{3}U_S$). The solution was found with a minimum square error: $k_e = 0.0249\,\frac{Vs}{rad}$, $L = 0.0020\,H$.

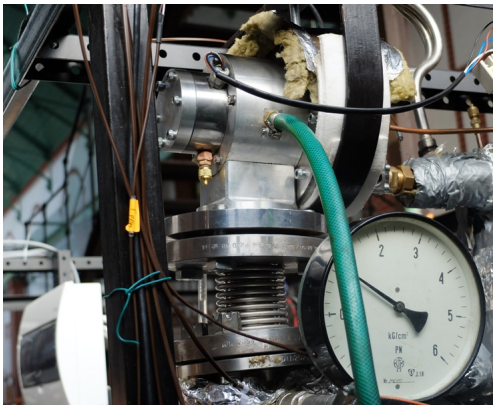

Figure 6: Vapour microturbine set during test runs

The values of the isentropic enthalpy drop of air were calculated from the relation:

$$H_s = C_p T_1 \left[1 - \left(\frac{p_2}{p_1} \right)^{\frac{\kappa-1}{\kappa}} \right] \tag{21}$$

where C_p is a specific heat at a constant pressure, κ is an isentropic exponent.

The values of the isentropic enthalpy drop of the vapour of the ethanol were taken from the RefProp database.

Turbine coefficients k_1, k_2 were calculated from equation 19. The following values were determined: $k_1 = 2.9022 \cdot 10^{-9}\, m^2 s$, $k_2 = 1.2500 \cdot 10^{-10}\, \frac{m^3 s}{rad}$ (for the compressed air operation) and $k_1 = 3.4103 \cdot 10^{-9}\, m^2 s$, $k_2 = 1.5368 \cdot 10^{-10}\, \frac{m^3 s}{rad}$ (for the vapour of the ethanol operation).

The microturbine set rotor polar moment of inertia was also calculated (based on the geometrical dimensions and density of the rotor materials): $J = 0.00088\, kg\, m^2$.

A series of calculations were performed to compare the developed relations with the experimental examinations. The model was validated on a different set of observations than the ones used to determine the values of the model coefficients.

The rotational speed values were obtained by solving the equation 19. The values of the current intensity and voltage were calculated from the

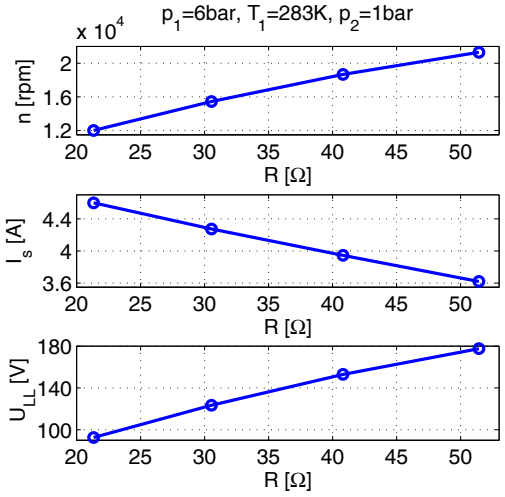

Figure 7: Rotational speed n, phase current intensity I_s and phase-to-phase voltage U_{LL} as a function of load resistance R with compressed air as a working medium, obtained from the experiment, for inlet pressure $p_1 = 6\,bars$, inlet temperature $T_1 = 283\,K$ and outlet pressure $p_2 = 1\,bar$

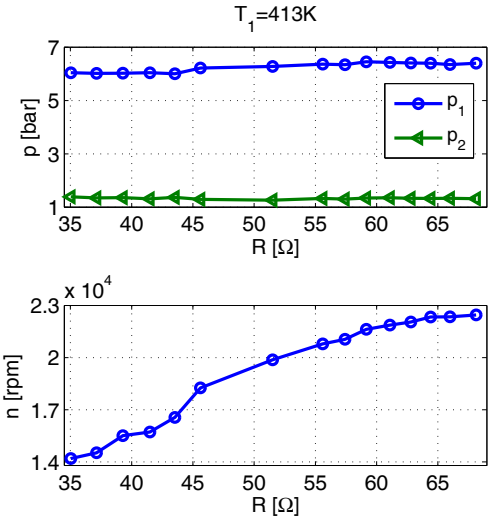

Figure 8: Inlet pressure p_1, pressure p_2 after the turbine and rotational speed n as a function of load resistance R with a vapour of ethanol as a working medium, obtained from the experiment, for inlet temperature $T_1 = 413\,K$

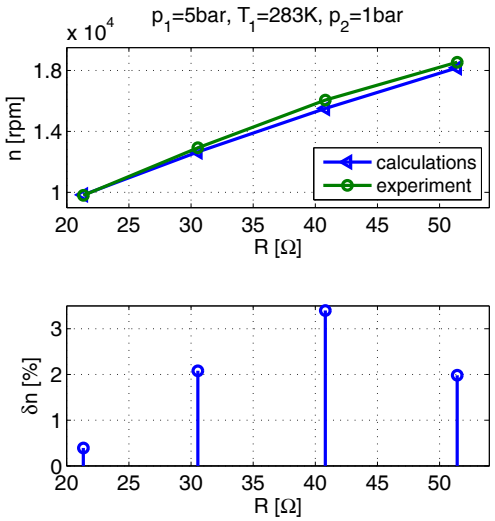

Figure 9: Rotational speed n as a function of load resistance R with compressed air as a working medium and relative errors δn between the experiment and calculations, for inlet pressure $p_1 = 5\,bars$, inlet temperature $T_1 = 283\,K$ and outlet pressure $p_2 = 1\,bar$

relations:

$$I_s = \frac{p\omega k_e}{\sqrt{\left(\frac{\pi^2 R}{18} + R_s\right)^2 + (p\omega L)^2}} \tag{22}$$

$$U_{LL} = \frac{\pi^2\sqrt{3} I_s R}{18} \tag{23}$$

The sample results are shown in the diagrams. The input data for the calculations were experimentally recorded values of the working medium parameters and load resistance. The resulting rotational speed, current intensity and voltage were compared with the experimental data.

Figs. 9, 10, 11 show the rotational speed, current intensity and voltage as a function of the load resistance, obtained from the experiment and calculations, for the compressed air operation, with the pressure at the turbine inlet and outlet equal to 5 bar and 1 bar respectively. The values of the relative differences between the results of the simulations and experiments are also shown in the graphs. The maximum values of the relative errors were 3.4 % for the rotational speed, 3.2 % for the current intensity and 3.5 % for the voltage.

A similar example, but this time for the vapour of alcohol as a working medium, is shown in Fig. 12. There are presented the experimentally ob-

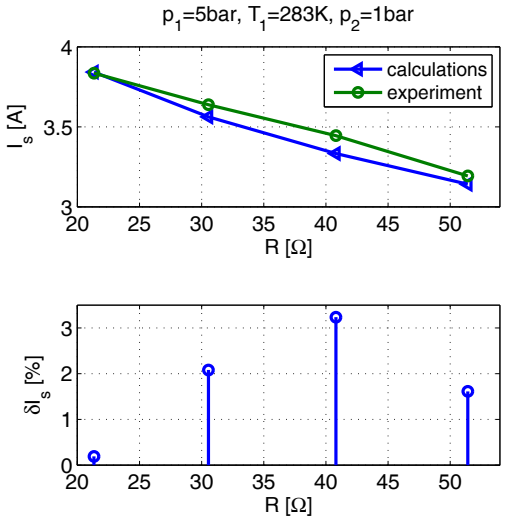

Figure 10: Phase current intensity I_s as a function of load resistance R with compressed air as a working medium and relative errors δI_s between the experiment and calculations, for inlet pressure $p_1 = 5\,bars$, inlet temperature $T_1 = 283\,K$ and outlet pressure $p_2 = 1\,bar$

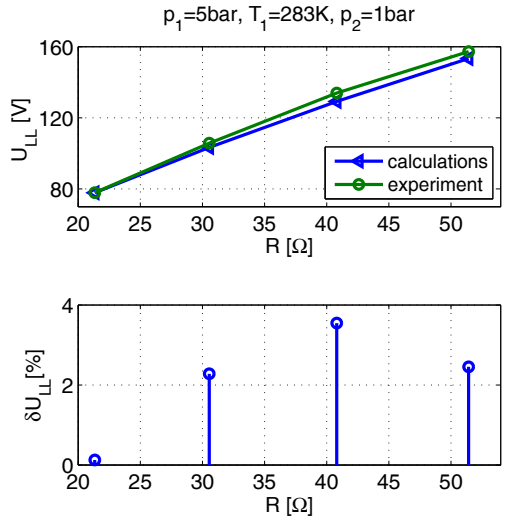

Figure 11: Phase-to-phase voltage U_{LL} as a function of load resistance R with compressed air as a working medium and relative errors δU_{LL} between the experiment and calculations, for inlet pressure $p_1 = 5\,bars$, inlet temperature $T_1 = 283\,K$ and outlet pressure $p_2 = 1\,bar$

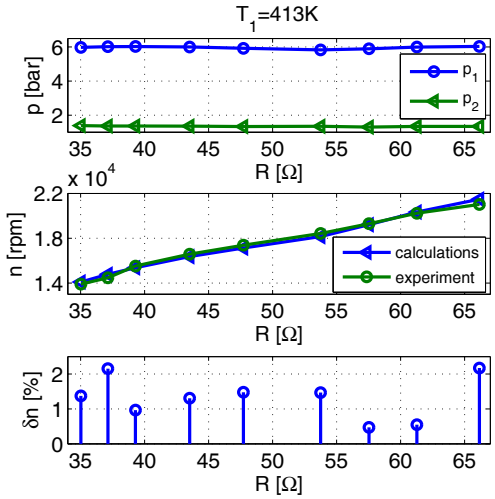

Figure 12: The rotational speed n as a function of load resistance R with a vapour of ethanol as a working medium and relative errors δn between the experiment and calculations, for inlet temperature $T_1 = 413\,K$

tained values of vapour pressure and rotational speed as a function of the load resistance. The mean values of the pressure during this test were 6.0 bar at the turbine inlet and 1.3 bar at the turbine outlet. The results of the rotational speed simulations and relative differences between the calculations and experiment were also shown. The maximum value of the relative error was 2.2 %.

The developed microturbine set model was also tested in unsteady operation conditions. Dynamical stages of operation were executed by changing the thermodynamic parameters of a working medium, or by changing the microturbine set load.

The test stand enables to record time histories of microturbine set operation parameters in the conditions of the step changes of the load resistance. Examples are presented in the graphs.

Figs. 13 shows the rotational speed, calculated and measured, after the step increase of the load resistance from 45 Ω to 56 Ω. During this test the microturbine worked with compressed air as a working medium. The mean value of the pressure at the inlet equalled 4.6 bar. After leaving the turbine, an air flowed directly to the environment. After the load change, the rotational speed increased gradually from 11900 rpm to 14160 rpm. The time after the load resistance change which was needed to reach the new steady

state was approximately equal to 16 seconds.

An example for the step decrease of load is presented in Fig. 14. This time vapour of alcohol was a working medium. The load resistance rapidly changed from 51 Ω to 43 Ω, at the mean values of the inlet pressure 6.2 bar and outlet pressure 1.0 bar. In this case, the changes of the rotational speed went in the opposite direction. The speed decreased gradually from 17700 rpm to 16180 rpm. The time needed for stabilisation of the microturbine set speed was approximately equal to 7 seconds.

It is noteworthy that the developed relations correctly predict the state of the microturbine set during the load resistance changes. The rotational speed values obtained from the calculations were close to those recorded experimentally.

In the example for the compressed air operation, the largest relative difference between the simulation and experiment was equal to 1.6 % (at about 4 seconds of the test). This transient difference between the experimental and the calculated results is difficult to explain from the point of view of the model. It might have been caused by the unstable operation of the bearings. The microturbine design predicted that the bearings should be lubricated with liquid ethanol. The compressed air tests were carried out without lubrication, which could have had a negative effect on the operation of the bearings. The mean value of the error during this test was equal to 0.6 %.

For the ethanol operation example, the largest and mean relative difference between the simulation and experiment were 2.4 % and 1.4 % respectively.

In Fig. 14, perturbations can be observed on the speed signal, especially visible after 6 seconds of the test. Such disturbances were observed during the experiment in certain ranges of rotational speeds. It can be assumed that these perturbations were the result of unpredictable interactions of the generator and the measuring system.

The performed calculations showed that the proposed model can also correctly predict the state of the microturbine set during inlet pressure dynamical changes.

Fig. 15 shows the microturbine set response to the rapid decrease in air pressure at the turbine inlet, from approximately 4.7 bar to 2.7 bar, while Fig. 16 shows a similar response after increasing the pressure from approximately 2.8 bar to 4.9 bar. In both tests, the microturbine set provided power for the electric energy receiver with 48 Ω resistance. In the first test, after a pressure change, the rotational speed decreased gradually from 12920 rpm to

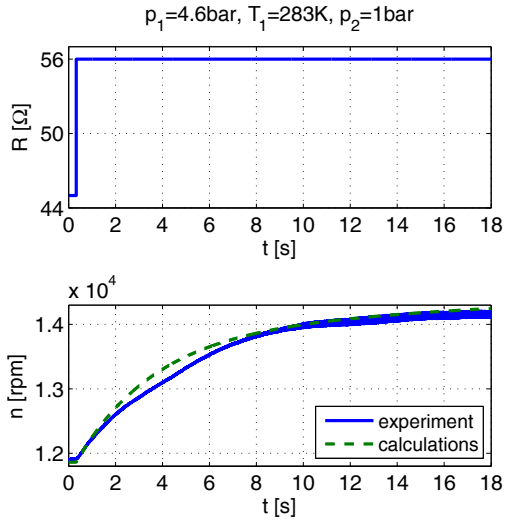

Figure 13: Rotational speed n as a function of time t, after load resistance R changes, with the compressed air as a working medium, obtained from the experiment and calculations, for inlet pressure $p_1 = 4.6\,bars$, inlet temperature $T_1 = 283\,K$ and outlet pressure $p_2 = 1\,bar$

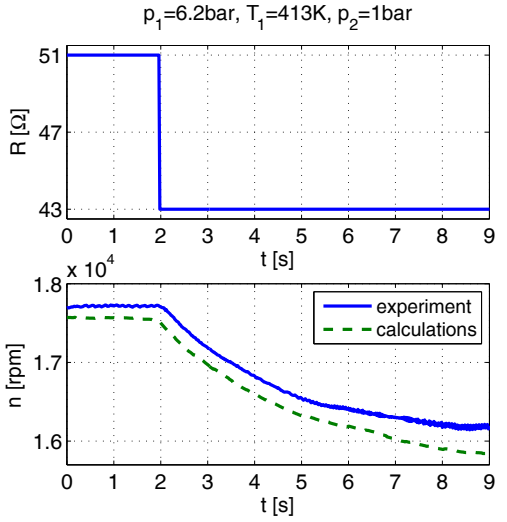

Figure 14: Rotational speed n as a function of time t, after load resistance R changes, with a vapour of ethanol as a working medium, obtained from the experiment and calculations, for inlet pressure $p_1 = 6.2\,bars$, inlet temperature $T_1 = 413\,K$ and outlet pressure $p_2 = 1\,bar$

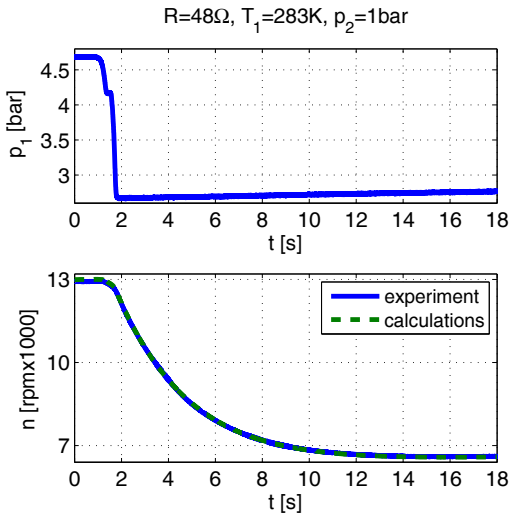

Figure 15: Rotational speed n as a function of time t, after pressure p_1 at the turbine inlet changes, with the compressed air as a working medium, obtained from the experiment and calculations, for load resistance $R = 48\,\Omega$, inlet temperature $T_1 = 283\,K$ and outlet pressure $p_2 = 1\,bar$

6610 rpm and in the second test increased from 6610 rpm to 13850 rpm. In both tests, the time needed for speed stabilisation was approximately equal to 15 seconds. In the first case, the speed time histories calculated and measured are so close that it is difficult to distinguish them on the graph. The largest relative difference between the simulation and experiment is equal to 0.6 % while the mean value of the error during this test is 0.2 %. For the second example. These values are 1.8 % and 0.7 % respectively.

During the experimental investigations described in [58] an attention was paid that relatively low-pressure pulsations of a medium before a microturbine clearly influences a rotational speed. The performed calculations show that the developed model can also correctly predict such phenomena. This is clearly visible in Fig. 17. It presents the measured inlet pressure, calculated and measured rotational speed as a function of time, with a vapour of ethanol as a working medium. In the turbine inlet pipeline, there were observed cyclically repeating pressure pulsations with the average amplitude of 0.08 bar and average frequency 0.4 Hz. Fluctuations of the same frequency, but delayed in the phase relative to the pressure pulsation of about 0.5 seconds, were observed in the rotational speed time histories. The average amplitude of the rotational speed fluctuations was 70 rpm. It can be observed

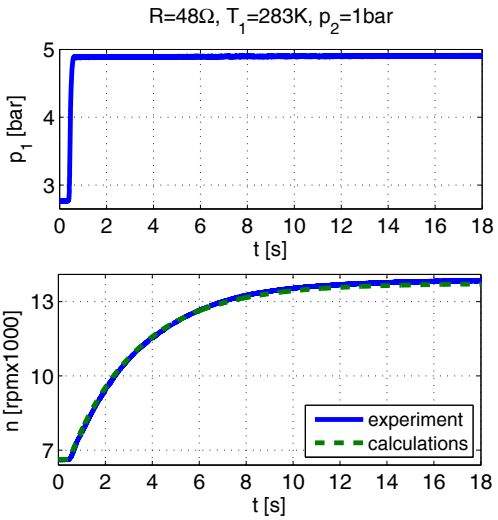

Figure 16: Rotational speed n as a function of time t, after pressure p_1 at the turbine inlet changes, with the compressed air as a working medium, obtained from the experiment and calculations, for load resistance $R = 48\,\Omega$, inlet temperature $T_1 = 283\,K$ and outlet pressure $p_2 = 1\,bar$

that the simulation calculations correctly predicted the amplitude and phase displacement of the microturbine set speed signal. The simulated time histories have slightly smaller values (an average of 2.4 %) than the measured one.

A number of factors could influence an inaccuracy of the presented simulations. Some of them may be related to the simplifications that the model introduces, a part undoubtedly results from an inaccuracy of the measurement system. It seems that the impact of the following factors should be discussed:

1. The systematic measurement errors had relatively small values (for example current intensity $\pm\,0.04\,\mathrm{A}$, voltage $\pm\,4.8\,\mathrm{V}$). Unfortunately, due to the individual character of the performed tests random errors have not been determined. These errors are caused by unknown and unpredictable changes in the experiment. These changes may occur in the measuring instruments, in the microturbine set or in the operating conditions.
2. The resistance measurement was carried out under a cold state. In fact, during an operation, resistors heated up and their resistance changed.

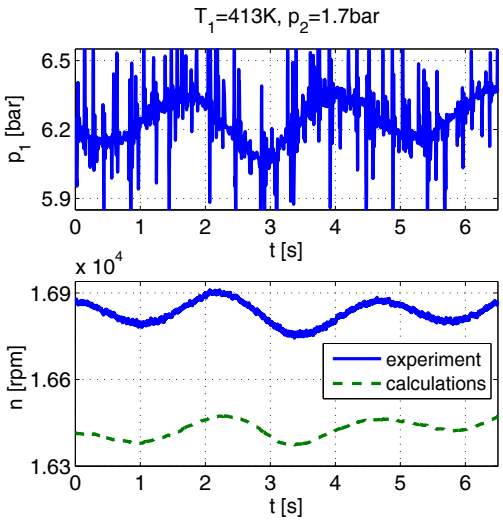

Figure 17: Rotational speed n as a function of time t, in the case of pressure p_1 pulsations at the turbine inlet, with a vapour of ethanol as a working medium, obtained from the experiment and calculations, for inlet temperature $T_1 = 413\,K$ and outlet pressure $p_2 = 1.7\,bars$

The value of these changes depends on several factors (current intensity, operation time, and ambient conditions) and it is difficult to determine. This phenomenon also applies to the generator stator resistance, which is additionally heated as a result of microturbine contact with hot vapour.

3. The turbine efficiency was approximated by a quadratic function. Theoretically, this is true for the gas path efficiency of an axial impulse stage with a zero degree of reaction [59], but turbine efficiency is also affected by stage internal losses. Until now, only the so-called cascade losses can be analytically determined. The theoretical determination of other internal losses, for example, leakage, rotor friction, partial admission losses etc., is not yet possible. In addition, the developed model does not take into account the mechanical losses in the microturbine set bearings.
4. The accuracy could increase if the power losses in the rectifier were taken into account. However, it would complicate the developed relations, because the complete model for the losses of a semiconducting device involves many variables capturing steady-state and transient behaviours [60].

5. The developed model assumes that the temperature at the turbine inlet is constant. In the example shown in section 2.1 (with the vapour of ethanol as a working medium). This simplification introduces to 1 % inaccuracies. If the inaccuracy connected with this assumption was unacceptable (for example, due to the specific properties of the working medium), the model would have to be modified taking into account the effect of the changes in the inlet temperature. It can be expected that it would provide better matching the simulations with the experiments.

However, despite the mentioned factors, the obtained results show that the developed model provides sufficient (for typical engineering calculations) accuracy, comparable with the latest published results. For example, in the gas microturbine set models presented in [53] and [61] errors are less than 5 %. The vapour microturbine set model described in [56] ensures similar accuracy, but due to the adoption of a linear relation between a load resistance and a rotational speed, its area of reliable operation is much smaller.

4. Start-up operation

The simulation calculations were also performed for the start-up operations. It turns out that in this phase of the microturbine set operation the accuracy of the simulation results depends greatly on a type of working medium.

Fig. 18 presents the calculated and measured time histories of the rotational speed, during the start-up operation, with compressed air as a working medium. Compressed air was delivered from the gas cylinders filled with an auxiliary compressor. During the start-up phase, the valve at the turbine inlet was manually opened. The experimental speed signal is shown above approximately 2500 rpm because below this value the RPM measuring system is not effective. It can be observed, that in this case, the simulations correctly predicted the start-up process. The mean value of the relative error during the test was 2.6 %.

Before the start-up operation, with ethanol vapour as a working medium, the turbine was bypassed to obtain the required vapour parameters. After that the reducing valve at the bypass pipeline was closed, while, at the same time, opening the valve at the turbine inlet. Both the valves were manually adjusted. Due to the temperature of the working medium, the start-up velocity was limited in order to protect the microturbine elements from an excessive increase in the thermal stresses.

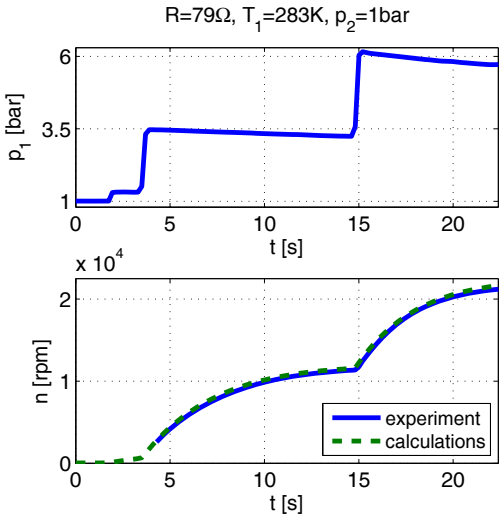

Figure 18: Rotational speed n as a function of time t during the start-up operation, with compressed air as a working medium, obtained from the experiment and calculations, for load resistance $R = 79\,\Omega$, inlet temperature $T_1 = 283\,K$ and outlet pressure $p_2 = 1\,bar$

An example of a start-up operation, with a vapour of ethanol as a working medium, is shown in Fig. 19. In this case, the accuracy of the simulation was definitely worse. During almost the entire start-up process, the calculated rotational speed was lower than the speed recorded during the experiment. The maximum value of the relative error was 104.9 % (in about 27 seconds of the test). Only after about 130 seconds, the calculated rotational speed approached the experimental values.

Such huge differences in the accuracy of the simulations between the examples in Figs. 18 and 19 have been interpreted as an effect of the thermal deformations of the turbine elements. As a result of the temperature changes, construction dimensions change, for example, clearances between a rotor and a turbine casing. The size of these clearances affects the value of turbine efficiency (especially in the case of a turbine stage with partial admission). The values of the model coefficients were determined at steady states, with a thermal state similar to the nominal. In the case of compressed air as a working medium (with a temperature close to the ambient). A thermal state of the turbine was not significantly dependent on an operation status. Thus, the developed model provides the correct results in the various operational states. The start-up in the Fig. 19 was performed from the cold

state turbine. The temperature of a vapour of ethanol at the turbine inlet was approximately 140 ^{o}C. It can be concluded that clearances values differ significantly between the cold and hot turbine state. Thus, the acceptable calculation accuracy was obtained only after the turbine reached the appropriate thermal state. This is confirmed by the example in Fig. 20. This is the start-up process with ethanol as a working medium. Before this test, the microturbine set was operating for a long time and was stopped for the purpose of replacing the load resistance. It can, therefore, be concluded that the start-up was performed from a warm state. In this case, the accuracy of the calculations has definitely increased. The maximum value of the relative error during the start-up operation was 25.0 %. Already after about 20 seconds, the calculated speed approached the experimental values.

The completed calculations show that an accuracy of simulations is related to a thermal state of a turbine. The highest accuracy is obtained when simulations are related to conditions in which a thermal state of a turbine is close to that at which the values of the model coefficients have been determined. After changing a thermal state, an accuracy may decrease. The experience collected during the described research indicates, that in a case of sets operating in ORC installations, this phenomenon can be expected in a start-up operation from a cold state. The negative effect of this phenomenon is definitely lower for working mediums at a temperature close to an ambient. In such cases, a thermal condition of a turbine does not change so significantly during operation.

5. Conclusions

This paper presents the mathematical model of a set consisting of a vapour microturbine, three-phase permanent magnet generator and diode rectifying unit. The developed relations result from the generic equations.

The model parameter values were determined based on the experimental data. The data for the two different working medium were used (compressed air and vapour of ethanol).

A series of calculations were performed to simulate the performance of the examined microturbine set in conditions, similar to those expected to take place in real operation. Steady as well as unsteady states (load or working medium pressure changes) were analysed. The simulation data were compared with the results of the experimental examination of the microturbine set. Within a wide range of operation area the results of the simulations

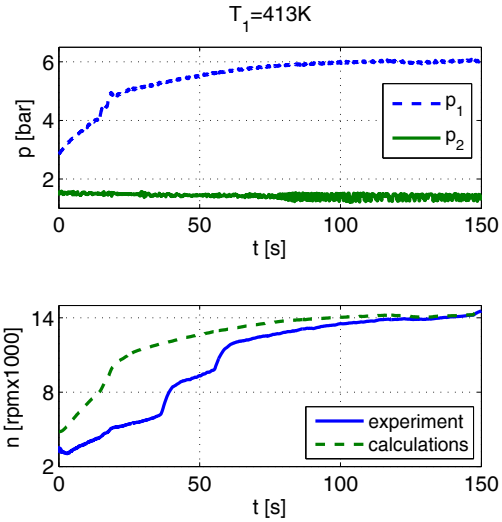

Figure 19: Rotational speed n as a function of time t during the start-up operation from a cold state, with a vapour of ethanol as a working medium, obtained from the experiment and calculations, for inlet temperature $T_1 = 413\,K$

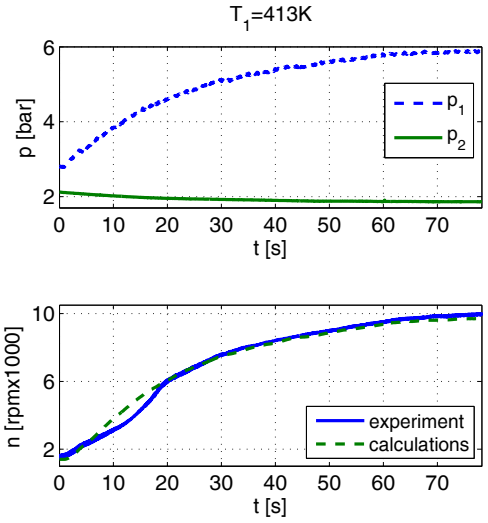

Figure 20: Rotational speed n as a function of time t during the start-up operation from a warm state, with a vapour of ethanol as a working medium, obtained from the experiment and calculations, for inlet temperature $T_1 = 413\,K$

were close to the experimental data. The relative differences between the experiment and the model results did not exceed 5 %. The possible reasons for the errors were noticed and discussed.

The developed model ensures comparable accuracy as gas microturbine models found in the literature. In the case of the vapour microturbine sets, in addition to accuracy, it provides a larger area of operation.

The simulations were also performed for start-up operations. It turns out that in this phase the accuracy of the simulation results depended greatly on a thermal state of a microturbine.

The presented model neglecting the temperature change at the turbine inlet. This simplification limits the area of a reliable operation of the microturbine set model. The paper indicates how the model could be modified if the inaccuracy were unacceptable. However, such a modification of the model would not solve the problem of inaccuracies in the simulation in a start-up operation from a cold state.

The developed model can be a useful tool for some engineering applications or for studying the various operational aspects of vapour microturbine sets. Moreover, the provided unique experimental data are the added value to the state of the art related to vapour microturbines. A combination of theoretical considerations with operational data of the real device will bridge the gaps between research, development and implementation.

Acknowledgements

This research did not receive any specific grant from funding agencies in the public, commercial, or non-profit sectors.

References

[1] C. A. Oberst, H. Schmitz, R. Madlener, Are prosumer households that much different? evidence from stated residential energy consumption in germany, Ecological Economics 158 (2019) 101–115. doi:10.1016/j.ecolecon.2018.12.014.

[2] Y. Zhu, F. Wang, J. Yan, The potential of distributed energy resources in building sustainable campus: The case of sichuan university, Energy Procedia 145 (2018) 582–585. doi:10.1016/j.egypro.2018.04.085.

[3] O. Dumont, R. Dickes, M. D. Rosa, R. Douglas, V. Lemort, Technical and economic optimization of subcritical, wet expansion and transcritical organic rankine cycle (orc) systems coupled with a biogas power plant, Energy Conversion and Management 157 (2018) 294–306. doi:10.1016/j.enconman.2017.12.022.

[4] J. Wajs, D. Mikielewicz, Effect of surface roughness on thermal-hydraulic characteristics of plate heat exchanger, Key Engineering Materials 597 (2013) 63–74. doi:10.4028/www.scientific.net/KEM.597.63.

[5] J. Wajs, D. Mikielewicz, E. Fornalik-Wajs, Thermal performance of a prototype plate heat exchanger with minichannels under boiling conditions, Journal of Physics: Conference Series 745 (2016) 63–74. doi:10.1088/1742-6596/745/3/032063.

[6] H. Wang, R. B. Peterson, Performance enhancement of a thermally activated cooling system using microchannel heat exchangers, Applied Thermal Engineering 31 (14) (2011) 2951–2962. doi:10.1016/j.applthermaleng.2011.05.026.

[7] J. S. Pereira, J. B. Ribeiro, R. Mendes, G. C. Vaz, J. C. André, Development of a direct concept helical-coil evaporator for an orc based micro-chp system, Energy Procedia 129 (2017) 474–478. doi:10.1016/j.egypro.2017.09.162.

[8] J. Wajs, D. Mikielewicz, E. Fornalik-Wajs, M. Bajor, Recuperator with microjet technology as a proposal for heat recovery from low-temperature sources, Archives of Thermodynamics 36 (2015) 49–64. doi:10.1515/aoter-2015-0032.

[9] T. Kura, E. Fornalik-Wajs, J. Wajs, Thermal and hydraulic phenomena in boundary layer of minijets impingement on curved surfaces, Archives of Thermodynamics 39 (2018) 147–166. doi:10.1515/aoter-2018-0008.

[10] J. Mascuch, V. Novotny, V. Vodicka, Z. Zeleny, Towards development of 1-10 kw pilot orc units operating with hexamethyldisiloxane and using rotary vane expander, Energy Procedia 129 (2017) 826–833. doi:10.1016/j.egypro.2017.09.196.

[11] J. Mascuch, V. Novotny, V. Vodicka, J. Spale, Z. Zeleny, Experimental development of a kilowatt-scale biomass fired micro – chp

unit based on orc with rotary vane expander, Renewable Energy-doi:10.1016/j.renene.2018.08.113.

[12] E. Yun, H. D. Kim, S. Y. Yoon, K. C. Kim, Development and characterization of small-scale orc system using scroll expander, Applied Mechanics and Materials 291-294 (2013) 1627–1630. doi:10.4028/www.scientific.net/AMM.291-294.1627.

[13] G.-D. Xia, Y.-Q. Zhang, Y.-T. Wu, C.-F. Ma, W.-N. Ji, S.-W. Liu, H. Guo, Experimental study on the performance of single-screw expander with different inlet vapor dryness, Applied Thermal Engineering 87 (2015) 34–40. doi:10.1016/j.applthermaleng.2015.05.006.

[14] F. Pantano, R. Capata, Expander selection for an on board orc energy recovery system, Energy 141 (2017) 1084–1096. doi:10.1016/j.energy.2017.09.142.

[15] J. Mikielewicz, M. Piwowarski, K. Kosowski, Design analysis of turbines for co-generating micro-power plant working in accordance with organic rankine's cycle, Polish Maritime Research (Special issue) (2009) 34–38. doi:10.2478/v10012-008-0042-4.

[16] T. Z. Kaczmarczyk, G. Żywica, E. Ihnatowicz, The impact of changes in the geometry of a radial microturbine stage on the efficiency of the micro chp plant based on orc, Energy 137 (2017) 530–543. doi:10.1016/j.energy.2017.05.166.

[17] L. Talluri, D. Fiaschi, G. Neri, L. Ciappi, Design and optimization of a tesla turbine for orc applications, Applied Energy 226 (2018) 300–319. doi:10.1016/j.apenergy.2018.05.057.

[18] A. Landelle, N. Tauveron, P. Haberschill, R. Revellin, S. Colasson, Organic rankine cycle design and performance comparison based on experimental database, Applied Energy 204 (2017) 1172–1187. doi:10.1016/j.apenergy.2017.04.012.

[19] C. Wang, J. Yan, C. Marnay, N. Djilali, E. Dahlquist, J. Wu, H. Jia, Distributed energy and microgrids (dem), Applied Energy 210 (2018) 685–689. doi:10.1016/j.apenergy.2017.11.059.

[20] J. Yan, Y. Zhai, P. Wijayatunga, A. M. Mohamed, P. E. Campana, Renewable energy integration with mini/micro-grids, Applied Energy 201 (2017) 241–244. doi:10.1016/j.apenergy.2017.05.160.

[21] A. Portoraro, M. Badami, M. Ferrero, Experimental tests of a small-scale microturbine with a liquid desiccant cooling system, International Journal of Energy Research 37 (2013) 1069–1078. doi:10.1002/er.2914.

[22] W. N. Macedo, L. G. Monteiro, I. M. Corgozinho, E. N. Macêdo, G. Rendeiro, W. Braga, L. Bacha, Biomass based microturbine system for electricity generation for isolated communities in amazon region, Renewable Energy 91 (2016) 323–333. doi:10.1016/j.renene.2016.01.063.

[23] K. Kosowski, K. Tucki, M. Piwowarski, R. Stepien, O. Orynycz, W. Włodarski, Thermodynamic cycle concepts for high-efficiency power plants. part b: Prosumer and distributed power industry, Sustainability 11 (2019) 26–47. doi:10.3390/su11092647.

[24] R. Amirante, P. Tamburrano, Novel, cost-effective configurations of combined power plants for small-scale cogeneration from biomass: Feasibility study and performance optimization, Energy Conversion and Management 97 (2015) 111–120. doi:10.1016/j.enconman.2015.03.047.

[25] M. Piwowarski, K. Kosowski, Design analysis of combined gas-vapour micro power plant with 30 kw air turbine, Polish Journal of Environmental Studies 23 (2014) 1397–1401.

[26] S. M. Bina, S. Jalilinasrabady, H. Fujii, Energy, economic and environmental (3e) aspects of internal heat exchanger for orc geothermal power plants, Energy 140 (2017) 1096–1106. doi:10.1016/j.energy.2017.09.045.

[27] M. Piwowarski, Design analysis of orc micro-turbines making use of thermal energy of oceans, Polish Maritime Research 20 (2013) 48–60. doi:10.2478/pomr-2013-0016.

[28] D. Mikielewicz, J. Wajs, P. Ziolkowski, J. Mikielewicz, Utilisation of waste heat from the power plant by use of the orc aided with bleed steam and extra source of heat, Energy 97 (2016) 11–19. doi:10.1016/j.energy.2015.12.106.

[29] D. Stepniak, M. Piwowarski, Analyzing selection of low-temperature medium for cogeneration micro power plant, Polish Journal of Environmental Studies 23 (4) (2014) 1417–1421.

[30] D. Mikielewicz, J. Wajs, J. Mikielewicz, Alternative cogeneration thermodynamic cycles for domestic orc, Chemical and Process Engineering 39 (2018) 75–84. doi:10.24425/119100.

[31] L. Jiang, H. Lu, L. Wang, P. Gao, F. Zhu, R. Wang, A. Roskilly, Investigation on a small-scale pumpless organic rankine cycle (orc) system driven by the low temperature heat source, Applied Energy 195 (2017) 478–486. doi:10.1016/j.apenergy.2017.03.082.

[32] J. Wajs, D. Mikielewicz, B. Jakubowska, Performance of the domestic micro orc equipped with the shell-and-tube condenser with minichannels, Energy 157 (2018) 853–861. doi:10.1016/j.energy.2018.05.174.

[33] K. Kosowski, R. Stepien, W. Wlodarski, M. Piwowarski, L. Hirt, Partial admission stages of high efficiency for a microturbine, Journal of Vibrational Engineering and Technologies 2 (2014) 441–448.

[34] Y. Fershalov, A. Y. Fershalov, M. Y. Fershalov, Microturbine with new design of nozzles, Energy 157 (2018) 615–624. doi:10.1016/j.energy.2018.05.153.

[35] E. Sauret, Y. Gu, Three-dimensional off-design numerical analysis of an organic rankine cycle radial-inflow turbine, Applied Energy 135 (2014) 202–211. doi:10.1016/j.apenergy.2014.08.076.

[36] W. Włodarski, Control of a vapour microturbine set in cogeneration applications, ISA Transactionsdoi:10.1016/j.isatra.2019.04.028.

[37] G. Zywica, P. Bagiński, Investigation of gas foil bearings with an adaptive and non-linear structure, Acta Mechanica et Automatica 13 (2019) 5–10. doi:10.2478/ama-2019-0001.

[38] I. Hernandez-Carrillo, C. J. Wood, H. Liu, Advanced materials for the impeller in an orc radial microturbine, Energy Procedia 129 (2017) 1047–1054. doi:10.1016/j.egypro.2017.09.241.

[39] M. J. Kim, J. H. Kim, T. S. Kim, The effects of internal leakage on the performance of a micro gas turbine, Applied Energy 212 (2018) 175–184. doi:10.1016/j.apenergy.2017.12.029.

[40] A. Cavarzere, M. Morini, M. Pinelli, P. R. Spina, A. Vaccari, M. Venturini, Experimental analysis of a micro gas turbine fuelled with vegetable oils from energy crops, Energy Procedia 45 (2014) 91–100. doi:10.1016/j.egypro.2014.01.011.

[41] P. Saiai, S. Chaitep, D. Bundhurat, P. Watanawanyoo, An experimental investigation of vapor generator characteristics in a low-pressure turbine engine, Indian Journal of Science and Technology 7 (8) (2014) 1130–1136.

[42] A. Cagnano, E. D. Tuglie, On-line identification of simplified dynamic models: Simulations and experimental tests on the capstone c30 microturbine, Electric Power Systems Research 157 (2018) 145–156. doi:10.1016/j.epsr.2017.12.006.

[43] K. Kosowski, W. Wlodarski, M. Piwowarski, R. Stepien, Performance characteristics of a micro-turbine, J Vib Eng Technol 2 (2014) 341–350.

[44] G. Żywica, T. Z. Kaczmarczyk, E. Ihnatowicz, T. Turzyński, Experimental investigation of the domestic chp orc system in transient operating conditions, Energy Procedia 129 (2017) 637–643. doi:10.1016/j.egypro.2017.09.123.

[45] G. Pei, J. Li, Y. Li, D. Wang, J. Ji, Construction and dynamic test of a small-scale organic rankine cycle, Energy 36 (5) (2011) 3215–3223. doi:10.1016/j.energy.2011.03.010.

[46] Z. Domachowski, Specificity of automatic control of micro-turbines (steam or gas -driven and expanders) in dispersed generation system of heat and electric power, Polish Maritime Research (Special issue) (2009) 9–13. doi:10.2478/v10012-008-0038-0.

[47] A. E. Ruano, P. J. Fleming, C. A. Teixeira, K. Rodríguez-Vázquez, C. M. Fonseca, Nonlinear identification of aircraft gas-turbine dynamics, Neurocomputing 55 (2003) 551–579. doi:10.1016/S0925-2312(03)00393-X.

[48] S. Bracco, F. Delfino, A mathematical model for the dynamic simulation of low size cogeneration gas turbines within smart microgrids, Energy 119 (2017) 710–723. doi:10.1016/j.energy.2016.11.033.

[49] S. Nayak, D. Gaonkar, Modeling and performance analysis of microturbine generation system in grid connected/islanding operation, International Journal of Renewable Energy Research 2 (4) (2012) 750–757.

[50] M. Razaghi, S. Hosseinalipour, E. Abdolahi, Static and dynamic mathematical modeling of a micro gas turbine, Journal of Mechanics 29 (2013) 327–335. doi:10.1017/jmech.2013.3.

[51] Y. Zhu, K. Tomsovic, Development of models for analyzing the load-following performance of microturbines and fuel cells, Electric Power Systems Research 62 (1) (2002) 1–11. doi:10.1016/S0378-7796(02)00033-0.

[52] X. Xu, K. Li, F. Qi, H. Jia, J. Deng, Identification of microturbine model for long-term dynamic analysis of distribution networks, Applied Energy 192 (2017) 305–314. doi:10.1016/j.apenergy.2016.08.149.

[53] M. Badami, M. G. Ferrero, A. Portoraro, Dynamic parsimonious model and experimental validation of a gas microturbine at part-load conditions, Applied Thermal Engineering 75 (2015) 14–23. doi:10.1016/j.applthermaleng.2014.10.047.

[54] H. Asgari, X. Chen, M. B. Menhaj, R. Sainudiin, Artificial neural network–based system identification for a single-shaft gas turbine, Journal of Engineering for Gas Turbines and Power 135 (2013) 1–7. doi:10.1115/1.4024735.

[55] G. L. Martins, S. L. Braga, S. B. Ferreira, Design optimization of partial admission axial turbine for orc service, Applied Thermal Engineering 96 (2016) 18–25. doi:10.1016/j.applthermaleng.2015.09.041.

[56] W. Włodarski, Experimental investigations and simulations of the microturbine unit with permanent magnet generator, Energy 158 (2018) 59–71. doi:10.1016/j.energy.2018.05.199.

[57] G. Wood, M. Newborough, Dynamic energy-consumption indicators for domestic appliances: environment, behaviour and design, Energy and Buildings 35 (8) (2003) 821–841. doi:10.1016/S0378-7788(02)00241-4.

[58] K. Kosowski, M. Piwowarski, R. Stepien, W. Włodarski, Design and investigations of the ethanol microturbine, Archives of Thermodynamics 39 (2018) 41–54. doi:10.1515/aoter-2018-0011.

[59] K. Kosowski, Steam and Gas Turbines, Alstom, 2007.

[60] Z. Xu, K. You, C. Zhang, Analytical models of power losses of a three phase ac-dc rectifier for hybrid electric vehicles, Energy Procedia 88 (2016) 978–984, cUE 2015 - Applied Energy Symposium and Summit 2015: Low carbon cities and urban energy systems. doi:10.1016/j.egypro.2016.06.122.

[61] P. Eguia, I. Zamora, E. Torres, J. S. Martín, M. Moya, J. Bruno, A. Coronas, Modelling and simulation of a microturbine during transient events, Energy Power Qual J 1 (2010) 354–359. doi:10.24084/repqj08.328.